Calorimetric analysis of coarse-grained polycrystalline aluminum by IRT and DIC

by L. Li[a], F. Latourte[b], J.-M. Muracciole[a,c], L. Waltz[a,c], L. Sabatier[a,c] and B. Wattrisse[a,c]

[a] Laboratoire de Mécanique et Génie Civil (LMGC), Montpellier 2 University, CNRS, France, *li.li@univ-montp2.fr*
[b] EDF R&D, MMC Dept., les Renardières, France
[c] Laboratoire de Micromécanique et d´Intégrité des Structures (MIST), IRSN-CNRS-Montpellier 2 University, France

Abstract

In the long term, this investigation aims at achieving grain scaled energy balances at finite strain in mechanically-loaded metallic polycrystal specimen. For this purpose, two complementary imaging techniques were used in order to investigate the so-called materials thermomechanical behaviour: Digital Image Correlation (DIC) and InfraRed Thermography (IRT) to investigate respectively the kinematic and the thermal response of the material and, combining these two techniques, its calorimetric response. The aim of this paper is to present and to validate a novel IRT method which allows to perform the local thermal field measurements. The validation procedure was performed on numerical example associated to aluminum polycrystalline aggregates.

1. Introduction

Polycrystalline materials are solids that are composed of an aggregate of crystalline grains of varying size and orientation. It is well known that, during a macroscopic monotonic tensile mechanical loading, the grain disorientation and the anisotropic nature of the crystal slips leads to a heterogeneous plastic deformation [1, 2], and consequently to a heterogeneous thermal distribution due to thermomechanical couplings effects or to plastically induced self-heating [3, 4].

Heterogeneous phenomena on mechanical and thermal fields have been widely studied using imaging techniques such as InfraRed Thermography (IRT) since the end of the 1970s [5, 6], and Digital Image Correlation (DIC) since the last two decades [7]. With the progress achieved in the fields of optical techniques associated with quantitative image processing, the quality and precision of displacement and temperature full-field measurements have tremendously increased in the last decade. At the same time, the development of automated Electron BackScattered Diffraction (EBSD) imaging techniques has contributed to a better monitoring of the microstructure evolution during plastic strain [8, 9, 10].

Grain scale experimental energy balances are necessary to access the local transformation energy evolution, so as to contribute to a better knowledge of the local thermomechanical signature of the material deformation mechanisms, and in the end to propose thermomechanically consistent models of crystalline plasticity. The literature reports only a few works devoted to the experimental determination of energy balances at the scale of the grain in metallic materials [11, 12, 13, 14, 15, 16].

A novel IR data processing method is proposed in this paper to perform thermal and calorimetric measurements necessary to the construction of the local energy balance within each grain. The key feature of this method is that intergranular and intragranular effects can be considered explicitly in the data processing. The objective of this paper is to present and to validate this novel thermal data processing method, which allows us to evaluate the thermal behaviour of material at both a micro and macros scales.

2. Development of Constrained IRT method for thermal measurements

To establish the energy balance during a mechanical test, a coupled full-field kinematic and thermal measurements are performed. By construction, every imaging device records images in the Eulerian configuration. Afterwards, DIC algorithms applied to the visible images allow to build the kinematic transformation between the initial state and the current, deformed one. The IR camera records the temperature field of a deforming body in the Eulerian configuration during the mechanical loading. Therefore, in order to follow the thermal evolution of each material point of the targeted zone, we use the kinematic transformation obtained by DIC analysis to express the IR images in the Lagrangian configuration before the heat source computation as described in [6, 17, 14, 13, 16].

The microstructure of the specimen is determined through EBSD analysis. The grain scale kinematic measurements are determined with the Constrained DIC method presented in [18]. Knowing the displacement fields per grain

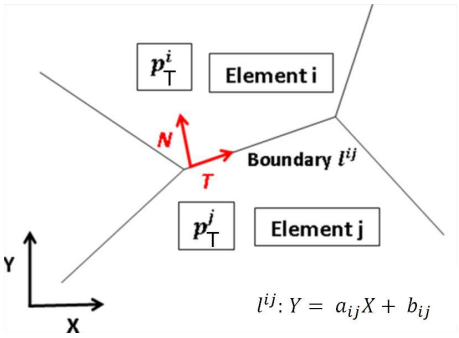

Figure 1: Description of the boundary between two adjacent elements i and j and the definition of the local coordinate system (N, T) of the boundary.

and the geometrical spatial matching between the CCD and the IR imaging system, the thermal data provided by the IR camera were linearly spatially interpolated for each acquisition time using the deformed configuration position given by the Constrained DIC computation. This operation allows to track material particle associated with the DIC computational mesh, and thus enables to construct the "microstructural" IR images in the Lagrangian configuration [6, 17, 16].

The IR camera records thermal radiations of the observed surface, and a pixel calibration protocol described in [19] is applied to determine the temperature field of the specimen induced by the mechanical loading.

2.1. Spatial discretization of the geometry

An unstructured mesh is applied within each grain of the microstructure in order to keep the representation of the physical grain boundaries. The smallest mesh unit within each grain is called "element", and each element is constituted by a set of pixels localized within a polygon. The elements' boundaries are accurately determined and retained in order to apply specific adjacency condition with other elements.

2.2. Thermal restricting constraint

A temperature shape function (Equation 1) is assigned to each element for the local thermal description.

$$u_T = f_T(X, Y, p_T) = \sum_{m=0}^{dm} \sum_{n=0}^{dn} \sum_{l=0}^{dl} \alpha_{mnl} X^m Y^n t^l \tag{1}$$

where, (X, Y) represents the IR coordinates in the Lagrangian configuration, t denotes the time and $p_T = \alpha_{mnl}$, is the parameter vector of the shape function.

The family of shape functions includes constant zero-order polynomial, multi-linear first-order polynomial and can be extended to second-order, quadratic, bi-quadratic and higher-order polynomial function. In order to account for increasingly complex thermal field, it is possible to use higher order shape function for the local description.

Once the shape function is chosen, different thermal continuity constraints can be introduced to describe the thermomechanical features of the material at the observation scale. The introduced restrictions deals always with along a given boundary l^{ij} between two adjacent elements i and j. As shown in Figure 1 with the local normal-tangential coordinate system (N, T) of the boundary l_{ij}, where

- The shape function for element i: $u_T^i = f_T(X_i, Y_i, p_T^i)$
- The shape function for element j: $u_T^j = f_T(X_j, Y_j, p_T^j)$
- The elements' boundary l^{ij} is modelled by a linear function: $Y = a_{ij}X + b_{ij}$,

The three following constrained conditions can be used together or independently to describe the different thermal features of the transformation:

- The continuity of the temperature can be introduced with the following restriction equation:

$$u_T^i = u_T^j \Longleftrightarrow f_T(X,Y,p_T^i) = f_T(X,Y,p_T^j) \qquad \forall (X,Y) \in l^{ij}$$

- The continuity of the normal temperature flow can be assured with the following restriction equation:

$$\nabla_N u_T^i = \nabla_N u_T^j \Longleftrightarrow \left(\begin{array}{c} \frac{\partial u_T^i}{\partial X} \\ \frac{\partial u_T^i}{\partial Y} \end{array} \right)_{X,Y} \overrightarrow{N}^{ij} = \left(\begin{array}{c} \frac{\partial u_T^j}{\partial X} \\ \frac{\partial u_T^j}{\partial Y} \end{array} \right)_{X,Y} \overrightarrow{N}^{ij} \qquad \forall (X,Y) \in l^{ij}$$

- The continuity of the tangential temperature flow can be imposed with the following restriction equation:

$$\nabla_T u_T^i = \nabla_T u_T^j \Longleftrightarrow \left(\begin{array}{c} \frac{\partial u_T^i}{\partial X} \\ \frac{\partial u_T^i}{\partial Y} \end{array} \right)_{X,Y} \overrightarrow{T}^{ij} = \left(\begin{array}{c} \frac{\partial u_T^j}{\partial X} \\ \frac{\partial u_T^j}{\partial Y} \end{array} \right)_{X,Y} \overrightarrow{T}^{ij} \qquad \forall (X,Y) \in l^{ij}$$

As the shape functions $f_T(X,Y,p_T^i)$ and $f_T(X,Y,p_T^j)$ are linear with respect to p_T^i and p_T^j, the above mentioned additional continuity constraints are linear equations in p_T^i and p_T^j, expressed as:

$$\left[\mathbf{A_{eq}^{ij}}\right] \left\{\mathbf{P_T^{ij}}\right\} = \{\mathbf{0}\}$$

Where, $\mathbf{A_{eq}^{ij}}$ is the elementary restriction matrix between element i and j, and $\mathbf{P_T^{ij}}$ is the elementary vector containing all the unknown parameter concerning the thermal shape function for the two elements p_T^i and p_T^j. This matrix is generally not square, its rank is necessarily smaller than the number of unknowns in vector $\mathbf{P_T^{ij}}$. This matrix $\mathbf{A_{eq}^{ij}}$ is triangulated in order to extract the independent equations and to build a new system that links the "dependant" unknowns of vector $\mathbf{P_T^{ij}}$ to the "independent" ones. The number of unknowns is thus restricted to the "independent" parameters. The other ones are deduced from these first ones by solving a linear system deduced from the triangulation process.

By iterating this operation for all the boundaries on which continuity constraints are applied, it is possible to construct a global restriction matrix for all the elements of the mesh with the imposed restrictions, as well as a global vector containing all the thermal parameters of all the elements. The fact of working in the Lagrangian framework, all the restriction matrices are determined one time throughout the data processing.

2.3. Solving the enriched thermal problem

As mentioned previously, the measured temperature fields are obtained using "Lagrangian thermography".

Afterwards the restricting continuity is added in these measured temperature fields, a least square optimization method is applied to minimise the gap between the measured temperature fields and the "constrained" ones, so as to construct the constrained temperature fields which respect the imposed restrictions. If the shape function u_T is time-dependant, a time smoothing is also performed in the same time in order to remove the temporal noise that appears in the IR measurements.

A reference unloaded specimen is also recorded by the IR camera during the test, in order to measure the temperature evolution of the room temperature. By subtraction, the temperature variation field $\theta(X,Y,t)$ of the specimen is obtained.

The 2D heat equation presented in [5, 20], obtained by integrating the heat equation over the sample thickness [21, 22]:

$$\left(\frac{\partial \theta}{\partial t} + v.grad\theta\right) + \frac{\theta}{\tau^{2D}} - \frac{k}{\rho C}\left(\frac{\partial^2 \theta}{\partial X^2} + \frac{\partial^2 \theta}{\partial Y^2}\right) = \frac{s}{\rho C} \tag{2}$$

The thermal shape function u_T is analytically differentiated in order to compute the time derivative and the Laplacian of the temperature field in each element. Generally, the spatial derivation is naturally performed in the Eulerian configuration. And, $(\frac{\partial \theta}{\partial t} + v.grad\theta)$ represents the particular time derivative of θ, which is equal to the

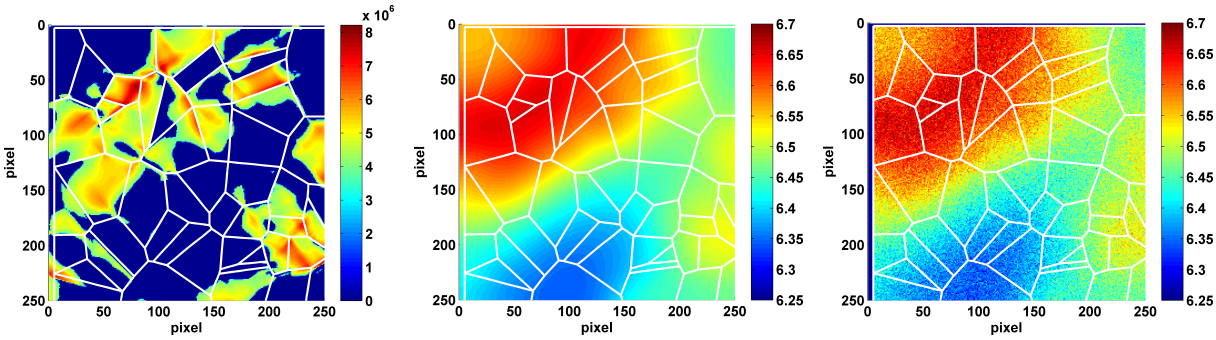

(a) Local theoretical heat source field, w_{ch}^{th} in W/m^3.

(b) Theoretical temperature variation field, θ^{th} in K.

(c) Noisy temperature variation field, θ^{noisy} in K.

Figure 2: Theoretical heat source field for COMSOL Multiphysics and the theoretical and the noisy temperature variation field.

partial time derivative $\dot{\theta}$ in the Lagrangian configuration [6, 17]. Thus, after all these heat source computations for each element, a grain scale local heat source field could be deduced for each corresponding IR measurement.

Using this Constrained IR data processing method, different microstructural thermal problems can be treated depending on the different imposed restricting constraints. For instance,

- The less constrained configuration corresponds no continuity constraints at all between elements, which is suitable for describing the intragranular cracking behaviour of the polycrystalline aggregates.
- The most constrained situation is associated with the intergranular continuity, which corresponds to enforce the thermal continuity (temperature and temperature flow) at the boundaries of all elements, except the ones corresponding to the potential crack. In general, this configuration is much constrained to represent the complex thermal field.
- The intermediate situation consists in a imposed continuity on the boundaries of all elements belonging to a given grain. The thermal field is thus continuous within each grain but possibly discontinuous between two adjacent grains. This configuration is particularly suited to describe intragranular thermal heterogeneities and intergranular discontinuities.

In the following paper, the viability of this Constrained IR data processing method will be demonstrated through a numerical example associated to aluminum polycrystalline aggregates.

3. Numerical validation

With the purpose of validating the proposed methodology on heterogeneous thermal fields, it was chosen to use computer-generated thermal image associated to a completely known heat sources field.

3.1. Numerical thermal image generation

In order to obtain a heat source field compatible with the one obtained during the straining of an aluminum polycrystal, we have chosen to define the heat sources field as a function of the strain-rate field obtained by a Finite Element (FE) simulation on a given microstructure using a crystal plasticity law. The FE simulation was performed using code Aster for the Méric-Cailletaud crystal plasticity law [23] and for a given set of boundary conditions and grain orientations [24, 18].

The aim of this FE simulation is to provide realistic local kinematic fields associated to equilibrated stress fields. Afterwards, the simulated strain rate fields were then used to mimic a heat source field compatible with the development of localised plasticity within the grains, shown in Figure 2a, where the white lines represent the physical grain boundaries. Naturally, the generated heat sources does not respect the real energy balance of the material during the loading.

$\rho\ (kg/m^3)$	$C\ (J/kg/K)$	$k\ (W/m/K)$	$\tau_{th}^{2D}\ (W/m^2/K)$	$T_0^{ref}\ (K)$	$h_{contour}$	h_{grip}	$h_{surface}$
2700	950	200	25	300	25	100	25

Table 1: Table of the material thermophysical parameters and the heat transfer coefficient (h)

The strain rate evolution is exported from Code Aster and then imported in COMSOL Multiphysics. A pure thermal computation is then performed assuming homogeneous thermal properties of the specimen (see Table 1). The time-dependant problem is solved in two dimensions. The thermal boundary conditions correspond to convection exchanges on the left and right boundaries ($h_{contour}$ for the blue color boundaries in Figure 3), and the top and bottom boundaries (h_{grip} for the cyan color boundaries in Figure 3). Heat losses by convection are also taken into account on the whole specimen surface ($h_{surface}$).

The initial temperature is supposed to be homogeneous on the whole specimen surface. The thermal conditions between two a adjacent grains are perfect conduction, *i.e.* continuous temperature and heat flux. In order to mimic the acquisition of a series of images by an IR camera, the computed thermal field is sampled with a $100\ Hz$ frequency on a regular $256\ pixel \times 256\ pixel$ grid corresponding to an IR sensor, which is presented in Figure 2(b). The physical duration of the simulation is $6s$, which is consistent with real testing conditions.

A supplementary noise (white, centered, Gaussian with a $0.025K$ standard deviation) is added to mimic the thermal noise of the camera, shown in 2(c). This value is consistent with the specification of standard metrology cameras.

The thermal fields are computed using a purely thermal simulation, so the geometry of the specimen is kept constant throughout the simulation. The temperature fields are thus obtained in the "initial","reference" configuration, which gives directly the "Lagrangian" temperature maps. In order to get the "Eulerian" temperature maps, which are the ones that are in fact measured by IR cameras, it is possible to deform these temperature maps with the displacement fields associated with the mechanical simulation.

So as to focus "only" on the thermal aspects of the data processing, we will use here exclusively the "Lagrangian" temperature fields, thus supposing that the displacement field is perfectly known on the specimen surface. Naturally, errors in the displacement field measurements generate supplementary uncertainties in the heat sources estimation which are not studied in this paper.

3.2. Spatial discretization of the synthetic image

To perform a local thermal description, the geometry is meshed using quadratic quadrangular elements. Note that the mesh respects the geometry of the microstructure used for the simulation, and the magenta color represents the grains boundaries (see Figure 3).

For this numerical study, a spatial bi-quadratic and temporal linear shape function is assigned for each element, as shown in Equation 1, with $dm = dn = 2$ and $dl = 1$, and p_T is a vector with 18 parameters in each element.

3.3. Numerical results

Before the presentation of the numerical results, it is necessary here to clarify or recall some notions for this numerical investigation.

- Geometric mesh: (shown in Figure 3)
  - element: whose contours are in black color, is constituted by a set of pixels located within a polygon.
  - grain: whose contours are in magenta color, and all the elements inside a grain are constrained by the continuity restrictions.
- Shape function: $u_T(X, Y, t)$
  - in space: a bi-quadratic function.
  - in time: a linear function.

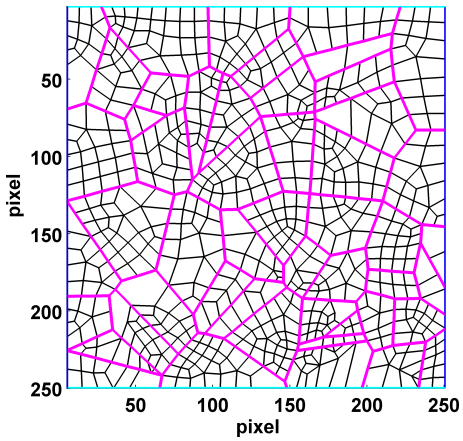

Figure 3: Computational mesh for IRT analysis

- Type of continuity:
  - continuity on temperature and on the temperature normal and tangential gradients
  - time: a time smoothing "window" of 60 IR images.
- Construction of the restriction matrix: all the continuities are valid for all the elements within each grain, there is no continuity between any grain.

The 600 noisy IR temperature variation maps ($100\ Hz$ during $6s$) were processed with all these data processing parameters, a constrained polynomial approximation is performed for each element, so as to deduce the fitted temperature variation maps respecting the continuity conditions. Afterwards, using the thermophysical material parameter shown in Table 1, the time derivative and the Laplacian of the fitted temperature variation field were determined for each element, and we obtained finally the corresponding heat source fields for each imposed noisy IR camera measurement.

Here, the instantaneous calculated thermal results (temperature and heat source) with the instantaneous errors are presented. For instance, the noisy temperature variation field shown in Figure 2c is taken as input of the procedure, the fitted temperature variation map shown in Figure 4a is obtained by the Constrained IR data processing method. After, the corresponding heat source field could be deduced, which is presented in Figure 4b.

Naturally, it is important de quantify the computation error for this data processing method. The error is defined by the the difference between the numerical calculated results with the imposed theoretical temperature and heat sources. Concerning the temperature variation field calculation, the residual between the "measured" noisy temperature variation field and the fitted one corresponds to the "noise" removed by the constrained data filtering. It is interesting to note, in Figure 5a, that this residual has the same histogram than the imposed noise, which suggests that only the imposed noise was suppressed by the data processing procedure. In additional, Figure 5b shows the almost null difference between the imposed theoretical temperature variation field θ^{th} and the fitted one θ^{fit}.

Knowing the temperature variation field were calculated element par element, thus it is possible to compared the averaged fields (temperature, heat sources), element per element or grain per grain. Figure 6a shows the average theoretic heat source field imported for the thermal simulation, and Figure 4b shows the corresponding one deduced par the Constrained IR data processing method, the difference is illustrated grain per grain in Figure 6b. The heterogeneity of the grain response is obviously and quantitatively observed, despite the strong diffusivity of the material.

4. Conclusion

In this paper, a specific thermal data processing method which fits the polycrystalline problem is presented. The comparison of thermal fields deduced by Constrained IR data processing method and imposed by FE simulation is

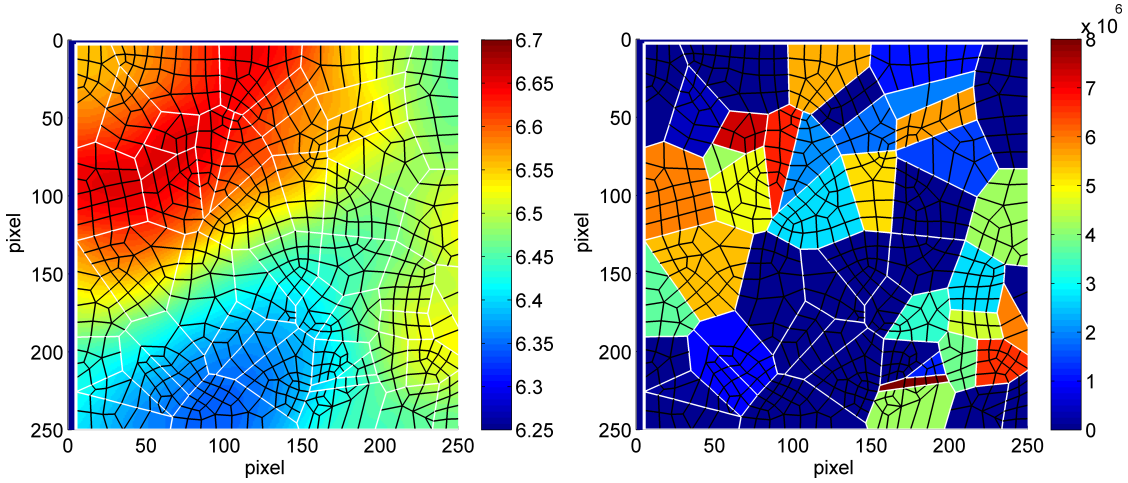

(a) The fitted temperature variation field, θ^{fit} in K.

(b) The calculated heat source field, w_{ch}^{fit} in W/m^3.

Figure 4: The calculated temperature variation field and the corresponding calculated grain averaged heat source field

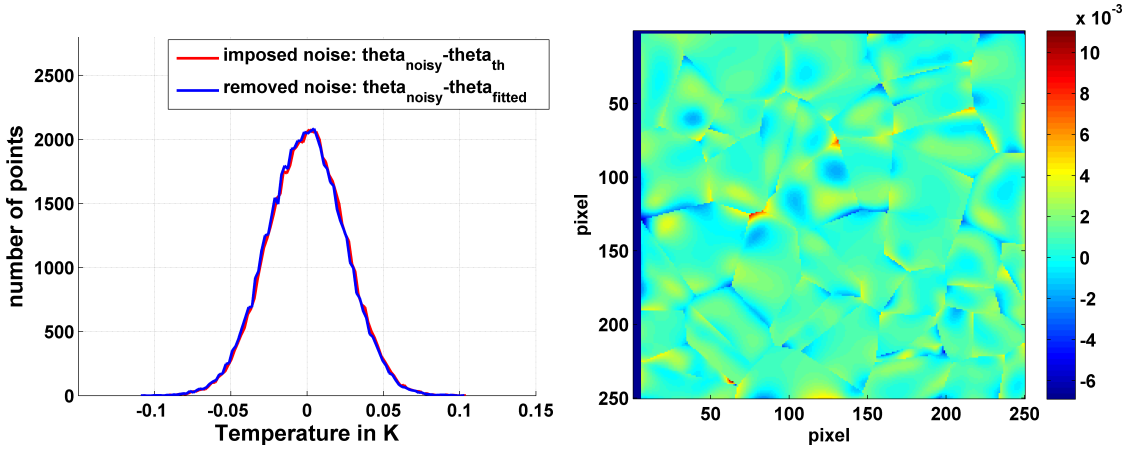

(a) The histogram of the imposed noise and the histogram of the removed noise by Constrained IRT method.

(b) The difference between the θ^{fit} and θ^{th} in K.

Figure 5: The histogram and the residual of the error for the temperature variation field estimation.

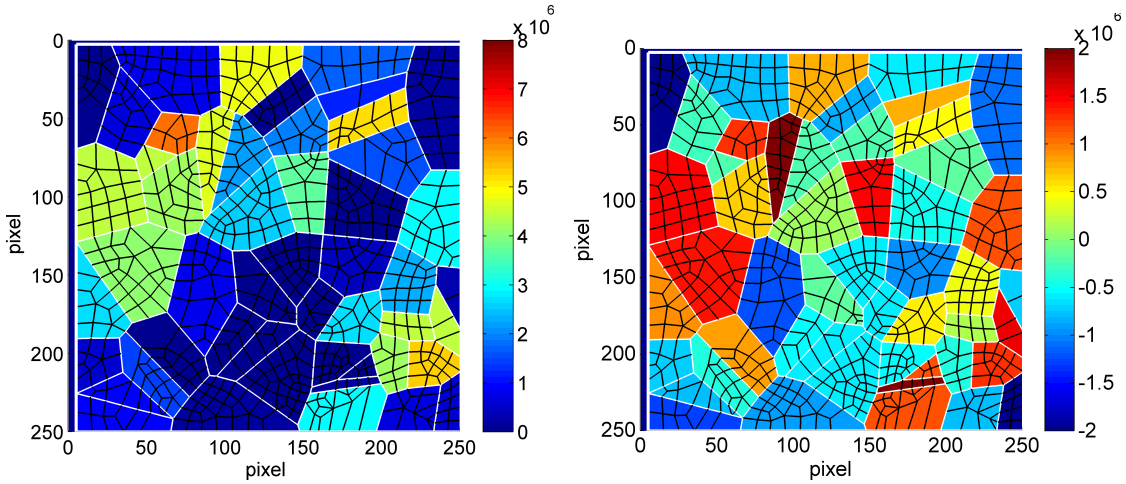

(a) The theoretical grain averaged heat source field, w_{ch}^{th} in W/m^3.

(b) The difference between the calculated and the theoretical heat source field in W/m^3.

Figure 6: The theoretical heat source field and the error for the heat source field estimation.

conclusive to validate our methodology. However, several possibilities are existing for the result improvement. For instance,

- A higher order shape function could be used for a accurate description of fine temperature gradients within each grain.
- A better temporal smoothing can be forced using higher order polynomials and larger temporal fitting windows for the amelioration of the heat source measurement.

The continuity conditions can be restrained in order to obtain more "flexible" temperature fields, by imposing the continuity constraints on a limited number of nodes on the boundary. All these formalisms can be adapted to impose discontinuity constrains on the temperature field or on the thermal gradients field in order to account for crack developmental.

In long term, this Constrained IR data processing method will be applied on an experimental test with the constrained DIC method [18], in order to obtain the different local thermomechanical variables and to build the grain scaled energy balances for each grain, so as to characterize the thermomechanical consistency of classical polycrystal plasticity modelling.

References

[1] B. Jaoul. *Étude de la plasticité et application aux métaux*. Dunod, 1965.

[2] W. Boas and M. E. Hargreaves. On the inhomogeneity of plastic deformation in the crystals of an aggregate. *Proceedings of the Royal Society of London. Series A. Mathematical and Physical Sciences*, 193(1032):89–97, 1948.

[3] W. S. Farren and G. I. Taylor. The heat developed during plastic extension of metals. *Proceedings of the Royal Society of London. Series A*, 107(743):422–451, 1925.

[4] G. I. Taylor and H. Quinney. The latent energy remaining in a metal after cold working. *Proceedings of the Royal Society of London. Series A*, 143(849):307–326, 1934.

[5] A. Chrysochoos. Energy balance for elastic plastic deformation at finite strain. *Journal of theoretical and applied mechanics*, Vol.4:p.589–614, 1985.

[6] A. Chrysochoos, B. Wattrisse, J.-M. Muracciole, and Y.EL. Kaim. Fields of stored energy associated with localiszed necking of steel. *Mechanics of Materials and Structures*, Volume 4, 2009.

[7] Bing Pan, Kemao Qian, Huimin Xie, and Anand Asundi. Two-dimensional digital image correlation for in-plane displacement and strain measurement: a review. *Measurement Science and Technology*, 20(6):062001, 2009.

[8] Brent L. Adams, Stuart I. Wright, and Karsten Kunze. Orientation imaging: The emergence of a new microscopy. *Metallurgical Transactions A*, 24:819–831, 1993.

[9] L Delannay, O.V Mishin, D.Juu Jensen, and P Van Houtte. Quantitative analysis of grain subdivision in cold rolled aluminium. *Acta Materialia*, 49(13):2441 – 2451, 2001.

[10] F.J. Humphreys. Review grain and subgrain characterisation by electron backscatter diffraction. *Journal of Materials Science*, 36:3833–3854, 2001.

[11] Z. Zhao, M. Ramesh, D. Raabe, A.M. Cuitino, and R. Radovitzky. Investigation of three-dimensional aspects of grain-scale plastic surface deformation of an aluminum oligocrystal. *International Journal of Plasticity*, 24(12):2278 – 2297, 2008.

[12] A. Saai, H. Louche, L. Tabourot, and H.J. Chang. Experimental and numerical study of the thermo-mechanical behavior of al bi-crystal in tension using full field measurements and micromechanical modeling. *Mechanics of Materials*, 42(3):275 – 292, 2010.

[13] C. Badulescu, M. Grédiac, H. Haddadi, J.-D. Mathias, X. Balandraud, and H.-S. Tran. Applying the grid method and infrared thermography to investigate plastic deformation in aluminium multicrystal. *Mechanics of Materials*, 43(1):36 – 53, 2011.

[14] L. Bodelot, E. Charkaluk, L. Sabatier, and P. Dufrénoy. Experimental study of heterogeneities in strain and temperature fields at the microstructural level of polycrystalline metals through fully-coupled full-field measurements by digital image correlation and infrared thermography. *Mechanics of Materials*, 43(11):654 – 670, 2011.

[15] Rian Seghir, Jean-François Witz, Laurence Bodelot, Eric Charkaluk, and Philippe Dufrénoy. An improved lagrangian thermography procedure for the quantification of the temperature fields within polycrystals. *Quantitative InfraRed Thermography Journal*, 10(1):74–95, 2013.

[16] Li Li, Jean Michel Muracciole, Laurent Sabatier, Laurent Waltz, and Bertrand Wattrisse. Analysis of the thermomechanical behavior of coarse-grained polycrystalline aluminum under tensile conditions. In *PhotoMechanics 2013*, Montpellier, France, 2013.

[17] A. Chrysochoos, V. Huon, F. Jourdan, J.-M. Muracciole, R. Peyroux, and B. Wattrisse. Use of full-field digital image correlation and infrared thermography measurements for the thermomechanical analysis of material behaviour. *Strain*, 46(1):117–130, 2010.

[18] Li Li, Latoure Félix, Jean Michel Muracciole, Laurent Waltz, Laurent Sabatier, and Bertrand Wattrisse. Capturing polycrystal plasticity and intergranular cracks with a novel DIC method. In *WCCM XI*, Barcelona, Spain, 2014.

[19] V. Honorat, S. Moreau, J.-M. Muracciole, B. Wattrisse, and A. Chrysochoos. Calorimetric analysis of polymer behaviour using a pixel calibration of an irfpa camera. *Quantitative InfraRed Thermography Journal*, 2(2):153–171, 2005.

[20] A. Chrysochoos, O. Maisonneuve, G. Martin, Caumon H., and J.C. Chezeaux. Plastic and dissipated work and stored energy. *Nuclear Engineering and Design*, 114:323–333, 1989.

[21] André Chrysochoos and Hervé Louche. An infrared image processing to analyse the calorific effects accompanying strain localisation. *International Journal of Engineering Science*, 38(16):1759 – 1788, 2000.

[22] Antoine Blanche. *Effets dissipatifs en fatigue à grand et très grand nombre de cycles*. These, Université Montpellier II - Sciences et Techniques du Languedoc, December 2012.

[23] L. Meric, P. Poubanne, and G. Cailletaud. Single crystal modeling for structural calculations. i, model presentation. *Journal of mechanical design (1990)*, 113(1):162–170, 1991. eng.

[24] F. Latourte, N. Rupin, and J.-M. Proix. Plasticité cristalline dans un acier bainitique revenu : simulations pour la validation de modèles à partir de mesures de champs. In *11e Colloque National en Calcul des Structures*, France, May 2013.